GEOLOGY

A multifault earthquake threat for the Seattle metropolitan region revealed by mass tree mortality

Bryan A. Black[1]*, Jessie K. Pearl[2]†, Charlotte L. Pearson[1], Patrick T. Pringle[3], David C. Frank[1], Morgan T. Page[4], Brendan M. Buckley[5], Edward R. Cook[5], Grant L. Harley[6], Karen J. King[5], Jonathan F. Hughes[7], David J. Reynolds[8], Brian L. Sherrod[2]

Compound earthquakes involving simultaneous ruptures along multiple faults often define a region's upper threshold of maximum magnitude. Yet, the potential for linked faulting remains poorly understood given the infrequency of these events in the historic era. Geological records provide longer perspectives, although temporal uncertainties are too broad to clearly pinpoint single multifault events. Here, we use dendrochronological dating and a cosmogenic radiation pulse to constrain the death dates of earthquake-killed trees along two adjacent fault zones near Seattle, Washington to within a 6-month period between the 923 and 924 CE growing seasons. Our narrow constraints conclusively show linked rupturing that occurred either as a single composite earthquake of estimated magnitude 7.8 or as a closely spaced double earthquake sequence with estimated magnitudes of 7.5 and 7.3. These scenarios, which are not recognized in current hazard models, increase the maximum earthquake size needed for seismic preparedness and engineering design within the Puget Sound region of >4 million residents.

INTRODUCTION

Earthquakes generated by the simultaneous rupture of multiple fault zones often define the worst-case seismic scenario for a given region (*1–4*). These events are infrequent and not often captured in the historic era, complicating efforts to identify where these compound earthquakes may occur and which faults are involved. Geological evidence such as fault scarps, landslides, subsidence, tsunami deposits, and fault-dammed lakes can extend earthquake histories thousands of years into the past (*5–9*). Yet, associated uncertainties typically span centuries to decades and are thus too broad to resolve these rapid earthquake-earthquake interactions (*10, 11*). This absence of historical benchmarks, combined with the lack of precise chronological constraints from the geological record, leaves major gaps in our understanding of the dynamics, configurations of fault linkages, and associated seismic risks of large, compound earthquake events.

A potential example of simultaneous or rapid rupture across fault zones occurs within the Puget Sound region of western Washington, USA, which includes the major metropolitan areas of Seattle, Tacoma, and Olympia. The Puget Sound region is seismically active and vulnerable to earthquakes from three sources: the Cascadia subduction zone (CSZ) megathrust, the deep intraplate (Benioff) zone, and a network of shallow faults in the North American Plate that are capable of rupturing to ground surface. Active shallow faults accommodate north-south contraction caused by oblique subduction of the Juan de Fuca Plate and clockwise rotation of the overriding plate (fig. S1) (*12, 13*). As many as 13 occur between ~47°N and the United States–Canadian border and have collectively produced dozens of moderate to large earthquakes over the past 16,000 years, but none have ruptured historically (*11*). Conventional radiocarbon dating shows that the shallow Seattle, Tacoma, Saddle Mountain, and Olympia fault zones produced earthquakes sometime between 780 and 1070 CE in what was the most prominent and widespread period of post-glacial activity within this fault network (Fig. 1) (*7, 10, 12, 14*). Dating uncertainties for these earthquakes overlap with one another across all four faults but span at least several decades in width. The most accurate radiocarbon age estimate places a large Seattle fault earthquake sometime between 900 and 930 CE, while uncertainties for the other three faults exceed 100 years (fig. S2) (*15–17*). Thus, questions have persisted as to whether fault systems involved in this ancient earthquake cluster are in some way linked and capable of rupturing in a single, large synchronous event or even in a rapid asynchronous series spanning months to decades (*6, 8, 12, 18–20*). Given the compounding impacts and additive energy releases involved in linked faulting, reducing dating uncertainties is critical to help establish realistic, geologically informed, worst-case seismic scenarios.

To further reduce dating uncertainties, dendrochronological analysis can pinpoint the calendar year, and even season, of fault rupture if trees killed by seismic activity remain preserved on the landscape (*21, 22*). The Puget Sound earthquake cluster approximately 1100 years ago induced landslides, uplifted fault scarps, and caused a local tsunami in Puget Sound, all of which drowned or buried trees at more than a dozen known locations spanning an area > 500 km² (*6, 8, 12*). On the Seattle fault zone, an earlier dendrochronological analysis revealed that trees drowned in a coseismic landslide into Lake Washington died the same dormant season as a tree buried in a tsunami deposit along the Puget Sound shoreline,

¹Laboratory of Tree Ring Research, University of Arizona, Tucson, AZ 85701, USA. ²U.S. Geological Survey Earthquake Science Center, Seattle, WA 98195, USA. ³Centralia College Department of Science, Centralia, WA 98531, USA. ⁴U.S. Geological Survey Earthquake Science Center, Pasadena, CA 91106, USA. ⁵Lamont-Doherty Earth Observatory, Columbia University, Palisades, NY 10964, USA. ⁶Department of Earth and Spatial Sciences, University of Idaho, Moscow, ID 83843, USA. ⁷School of Land Use and Environmental Change, University of the Fraser Valley, Abbotsford, BC V2S 7M8, Canada. ⁸Centre for Geography and Environmental Science, University of Exeter, Penryn Campus, Penryn, Cornwall TR10 9FE, UK.
*Corresponding author. Email: bryanblack@arizona.edu
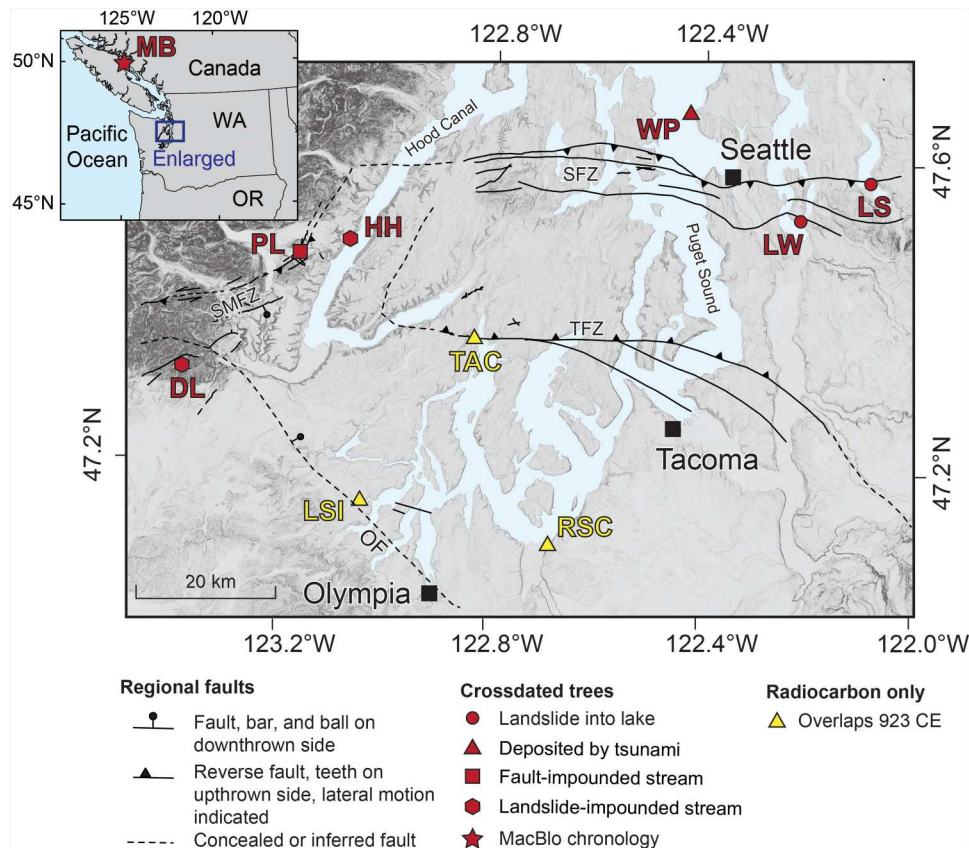†Present address: The Nature Conservancy, Tucson, AZ 85719, USA.

Fig. 1. Study region and sites. Inset: Regional setting spanning southwestern Canada to Washington and Oregon, USA. "MB" is the location of the "MacBlo" tree-ring chronology. Main map: Puget Sound region, principal fault locations (*19*), and study sites. SFZ, Seattle fault zone; SMFZ, Saddle Mountain fault zone; TFZ, Tacoma fault zone; OF, Olympia fault zone. "Crossdated trees" are sites where trees were sampled for this study: DL, Dry Bed Lake, PL, Price Lake, HH, Hamma Hamma, WP, West Point, LW, Lake Washington, LS, Lake Sammamish. "Radiocarbon only" are previously published radiocarbon dated earthquake sites with uncertainties that overlap 923 CE: LSI, Little Skookum Inlet, RCS, Red Salmon creek, TAC, Tacoma (see fig. S2 for radiocarbon ages). Map is adapted from (*12*).

revealing the widespread impacts of an earthquake approximately 1100 years ago, but did not establish an exact calendar year of the event or linkages with events on adjacent faults (*21*). In this study, we apply dendrochronological dating techniques to precisely link dates of tree death across six sites that span the Seattle and Saddle Mountain fault zones and anchor these earthquake-killed tree-ring chronologies with an absolutely dated chronology developed from live-collected trees. The exact calendar year of rupture is independently verified using a single-year cosmogenic radiocarbon pulse to tightly constrain linkages across these two shallow fault zones within the Puget Sound region.

RESULTS

Synchronous mortality of earthquake-killed trees

To precisely determine past earthquake timing and better understand rupture dynamics, we analyzed annual rings of subfossil Douglas-fir (*Pseudotsuga menziesii*) from six Puget Sound sites associated with the Seattle and Saddle Mountain fault zones (Fig. 1). Coseismic processes are believed to have killed the trees at all locations. Samples from multiple trees were obtained from Lake Washington (*n* = 16 trees, five with bark), east of Seattle, where a landslide from Mercer Island carried a standing forest to the lake floor and

drowned trees in 100-m of water (*21*); from the Hamma Hamma River delta area (*n* = 7 trees, two with bark) along Hood Canal, where a riparian forest drowned behind a landslide dam (*9*); and at Price Lake (*n* = 21 trees, four with bark) in the eastern Olympic Mountain foothills, where an upstream-facing scarp of the Saddle Mountain fault flooded a forest floor (*20*) (table S1). In addition, single trees were sampled from West Point, Seattle, where a tsunami deposited a bark-bearing log (*14*, *15*, *21*); lower Dry Bed Lake in the eastern Olympic Mountain foothills, formed when a rockslide-debris avalanche impounded the outflowing stream (*9*); and Lake Sammamish east of Seattle in a setting similar to the Lake Washington samples (*8*). At all three single-tree sites, samples retain a fully preserved outermost growth ring representing the final year of the tree's life (table S1). While it is possible that an earthquake on the Seattle fault zone could have caused the landslides, rock avalanches, and Puget Sound tsunami that killed trees at five of these sites, the trees at Price Lake could only have been killed by activity on the Saddle Mountain fault zone.

We matched ring-width patterns using well-established dendrochronology crossdating techniques (*23*) at Lake Washington, Hamma Hamma, and Price Lake. Tree-ring widths were then measured at a precision of 0.01 mm (*24*), after which a statistical check of crossdating accuracy was performed using the program COFECHA

(25). Each measurement time series was standardized to remove tree age/size-related trends and stand dynamics and thereby extract the interannual component of growth variability for dendrochronological dating (24). These standardized measurement time series were averaged into serially independent site-level chronologies suitable for correlation analysis. The single West Point, Dry Bed Lake, and Lake Sammamish samples were similarly measured along multiple radii, standardized, and then averaged into sample-level chronologies.

Ring-width patterns match not only within sites but also across sites. These matches are anchored by positive and significant Pearson correlation coefficients (r) among Lake Washington, Price Lake, and Hamma Hamma chronologies ($r = 0.42$, $P < 0.0001$: Hamma Hamma to Lake Washington; $r = 0.45$, $P < 0.0001$: Hamma Hamma to Price Lake; $r = 0.39$, $P < 0.001$: Price Lake to Lake Washington) when the outermost rings of bark-bearing trees are aligned with one another (Fig. 2A). Correlations at the position of bark alignment exceed all others when sliding site-level chronologies past one another in time in a running lead-lag analysis (Fig. 2, C to E). For lead-lag analysis, correlations are calculated as T values to mitigate the chances of spuriously high values when degrees of freedom are low, as could happen near the ends of overlapping time series (see Materials and Methods). The final tree ring at the three sites is complete, revealing that trees died during the same dormant season, which at these sites corresponds approximately to the months of October to March (26–28) (Fig. 2G).

To obtain exact calendar years for the Lake Washington, Price Lake, and Hamma Hamma chronologies, we averaged these three records and compared this regional mean with an absolutely dated reference chronology spanning 715 to 1990 CE. We assembled this reference chronology from 27 cores collected from live and dead old-growth Douglas-fir on MacMillan-Bloedel (MacBlo; now Weyerhauser) land on Vancouver Island some 280-km northwest of Seattle (Fig. 1). This chronology supersedes another from Vancouver Island as a regional reference for tree-ring dating (fig. S3) (29). The mean of the Lake Washington, Price Lake, and Hamma Hamma chronologies, when slid past the MacBlo chronology in a running lead-lag correlation analysis, has but one strong and unequivocal match that places the final growth year at all three locations to 923 CE (Fig. 2, B and F). The correlation with MacBlo is highly significant not only for the mean of the three sites ($r = 0.55$, $P < 0.0001$; Fig. 2B) but also for each of the individual sites ($r = 0.35$, $P = 0.0001$: Hamma Hamma and MacBlo; $r = 0.57$, $P < 0.0001$: Lake Washington and MacBlo; $r = 0.39$, $P = 0.0001$, Price Lake and MacBlo).

Independent dating verification using a cosmogenic radiocarbon pulse

To date these Puget Sound samples with a second, independent method, we analyzed individual tree-ring sequences for a jump in annual radiocarbon concentrations associated with an extreme solar proton event (30, 31). This rapid, large magnitude (~10‰) radiocarbon excursion between the years 774 and 775 CE is recorded globally in tree cellulose and can therefore be used as an exact geochronological anchor point (30, 32, 33). At Lake Washington, Price Lake, and Hamma Hamma, the largest single-year radiocarbon jump occurs at the crossdated years 774 to 775 CE, thereby
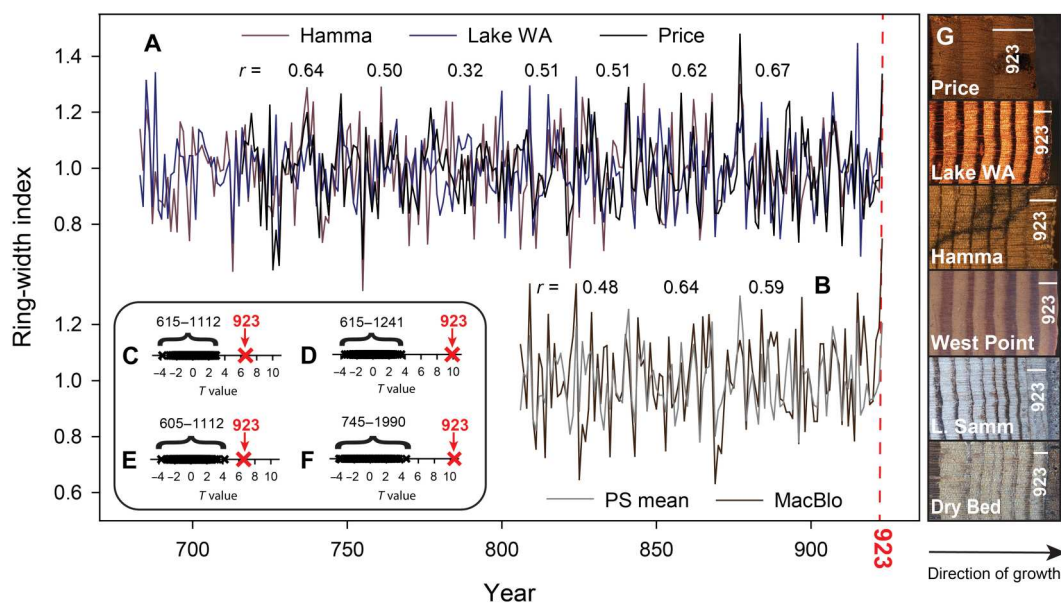
Fig. 2. Tree-ring dating of Puget Sound sites. (**A**) Site-level tree-ring width chronologies from Hamma Hamma, Lake Washington, and Price Lake. Numbers are running correlation coefficients (r) between each chronology and the mean of the other two, as calculated in 50-year windows overlapping by 25 years. (**B**) Mean of the three Puget Sound chronologies (PS mean) and the MacBlo chronology. Numbers are correlation running coefficients (r) between the plotted chronologies calculated in 50-year windows overlapping by 25 years. Inset: Heavy black horizontal bars represent the distribution of T values, a measure of correlation, when sliding each pair of chronologies back and forth through time relative to one another for (**C**) Hamma Hamma and Price Lake, (**D**) Hamma Hamma and Lake Washington, and (**E**) Lake Washington and Price Lake and (**F**) MacBlo and PS mean. T value when ends of chronologies are aligned to 923 is shown as a red "X." Values in brackets are the range of dates (CE) across, which chronologies are compared. (**G**) Images of the final tree rings from representative samples at all six sites. The final ring corresponds to 923 CE, the width of which is shown by a white line; bark is still attached to the bottom two samples.

confirming a final growth year of 923 CE at each site (Fig. 3). The timing of the maximum radiocarbon jump is identical to that published in other western North American datasets (fig. S4). At the Puget Sound sites, the initial rise in radiocarbon beyond 775 CE is relatively muted compared to other western North American sites. Such a response may be due to site- or species-specific biological carry-over effects, although is not without precedent, also occurring in mountain hemlock (*Tsuga mertensiana*) from Glacier Bay, Alaska (fig. S4) (*30*).

Synchrony with single-tree sites

Among the single-tree sites, the ring-width patterns from Dry Bed Lake and Lake Sammamish match those at Lake Washington, Price Lake, and Hamma Hamma in just one position, with the final ring at 923 CE (fig. S5, A and B). The West Point log was previously indicated to have died synchronously with Lake Washington trees, partly based on anatomical features (*21*). In our analysis, this log significantly correlates with Lake Washington ($r = 0.36$, $P < 0.0001$) and Hamma Hamma ($r = 0.38$, $P < 0.0001$) with a 923 CE end position. However, it correlates equally well with an end date of 764 CE (fig. S5C). The West Point log does not extend back to the 774 CE solar proton event, but radiocarbon "wiggle matching" constrains the last increment of the West Point log to 900 to 930 CE at greater than 95% confidence (*15*). Thus, the combination of evidence points to a 923 CE outermost ring for this sixth site.

DISCUSSION

Over the past several decades, earlier studies have documented widespread evidence of strong ground motions approximately 1100 years ago on the Saddle Mountain and Seattle fault zones as well as the locations of trees killed by these earthquakes in coseismic landslides, tsunamis, and stream impoundments (*6, 9, 18–20*). Now, tree-ring and annually resolved radiocarbon dating have pinpointed

Fig. 3. The 774–775 radiocarbon pulse in Puget Sound tree-ring data. Annual $\Delta^{14}C$ from tree samples of Hamma Hamma, Lake Washington, and Price Lake. Inset: Difference in $\Delta^{14}C$ from 1 year to the next to illustrate the magnitude of the jump from 774 to 775 CE (dashed vertical line). An enlarged symbol denotes the year of the largest radiocarbon jump in each time series, which at all three sites occurs from 774 to 775 CE.

the timing of Saddle Mountain and Seattle fault ruptures to within the same 6 months between late autumn of 923 CE through early spring of 924 CE, substantially reducing previous dating uncertainties that spanned decades or centuries (fig. S1). Under these updated constraints, ruptures can be explained either by two distinct earthquakes on two adjacent faults, or alternatively, by a single multifault earthquake. In the first of these cases, the two faults ruptured as two earthquakes separated by hours to months with a median magnitude for the Seattle fault zone estimated as moment magnitude (M_w) 7.5 (with M_w 7.3 and M_w 7.6 as the 5th and 95th percentiles) and a median magnitude for the Saddle Mountain fault zone of M_w 7.3 (with M_w 7.1 and M_w 7.5 as the 5th and 95th percentiles) (*11*). Modern earthquake series on this time scale include the New Madrid, USA, sequence in which mainshocks occurred on 16 December 1811, 23 January 1812, and 7 February 1812, and the December 1854 Ansei pair along Japan's Nankai subduction zone, in which mainshocks occurred 32 hours apart (*2–4*). A particularly close analog may be the 6 February 2023, southeast Türkiye Kahramanmaraş sequence in which a M_w 7.8 earthquake on the East Anatolian fault zone was followed 9 hours later by a M_w 7.5 earthquake on the adjacent Sürgü fault >20 km distant (*1*).

The second possibility is a single, larger, multifault earthquake rupturing both the Seattle and Saddle Mountain fault zones with a median magnitude estimated at M_w 7.8 (*11*). Simultaneous ruptures have occurred elsewhere in the modern record including the multifault 2001 M_w 7.9 Denali earthquake in southern Alaska, the 1992 M_w 7.3 Landers earthquake in southern California, and the 2016 M_w 7.8 Kaikōura, New Zealand earthquake, which involved more than 20 distinct faults (*3, 34, 35*). With a maximum interval of 180 days between ruptures, the statistics of earthquake size and triggering suggest the single multifault rupture scenario is about three times more likely than an earthquake doublet, although effects of fault geometry and connectivity, which remain poorly described for the two faults, could modify these probabilities (see Materials and Methods for details). In either the synchronous or asynchronous scenario, the Saddle Mountain and Seattle fault zones may be kinematically connected via a proposed master fault beneath the Puget Sound region (*19*), or a rupture on one fault could have transferred stress to or weakened the adjacent fault to produce a rapidly propagating earthquake sequence (*36*). Precise dating also strengthens evidence that, in this 923 to 924 CE instance, the Seattle and Saddle Mountain faults were not triggered by activity along the CSZ, for which the closest dates of rupture estimated from onshore evidence are 685 to 720 CE and 1035 to 1160 CE (*10*), both exclusive of 923 to 924 CE.

Our subannual temporal constraints on the Saddle Mountain and Seattle fault ruptures move the upper bound of possible hazard scenarios in the Puget Sound region. In a 2005 scenario for a modern M_w 6.7 Seattle fault earthquake, no fewer than 1600 lives are lost, nearly 10,000 buildings destroyed, and total economic losses approach $50 billion (*37*). A single linked earthquake across Seattle and Saddle Mountain faults at the median estimate of M_w 7.8 (*11*) would release approximately 38 times that amount of energy over a region spanning the eastern Olympic Mountain foothills through metropolitan Seattle while likely triggering a local tsunami (*14, 38*). In the alternative scenario of two closely timed earthquakes, infrastructure and landscape features weakened by rupture on the first fault would be especially vulnerable to the impacts of rupture on the second fault. Although the recurrence
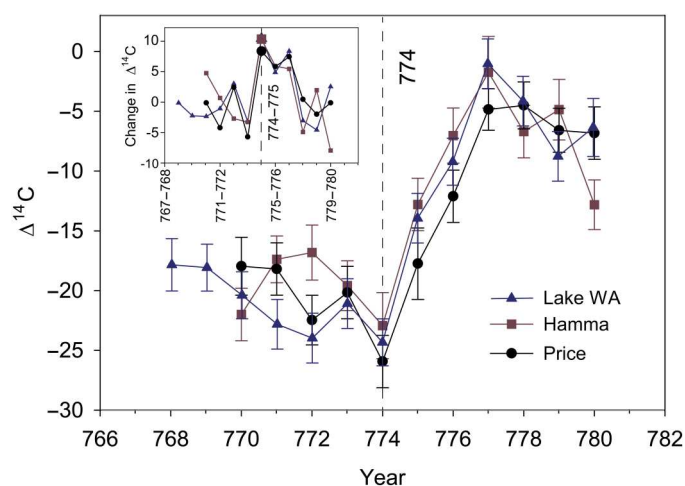
of such events remains unknown, they appear to be uncommon. Widespread coseismic landslides, rockslides, and a local tsunami suggest that the 923 to 924 CE earthquake was the most intense in the Puget Sound region since the end of the last glaciation approximately 16,000 years ago (7, 11).

Ultimately, the fine temporal resolution of our dating demonstrates close connectivity between the Seattle and Saddle Mountain fault zones and that ruptures along both can occur in rapid sequence. Yet, dendrochronology may also prove useful in revealing similar patterns of linked faulting at other locations in the Puget Sound region. For example, rupturing along the Seattle and Saddle Mountain fault zones could have been closely timed with rupturing along the Tacoma and Olympia fault zones, for which radiocarbon dating uncertainties of earthquake activity overlap 923 CE (Fig. 1 and fig. S1) (16, 17). Elsewhere in western North America, fault-adjacent trees could be used to identify pattern of linked ruptures along segments of the San Andreas fault or with segments of nearby faults (39, 40). On the CSZ, trees killed by subsidence revealed a rupture during the dormant season of 1699 to 1700 CE, a date later refined to 26 January 26 1700, from written records of tsunamis that reached Japan (22, 41). Killed trees, however, have only been sampled along 100 km of the 1100 km length of the subduction zone. Largely assumed to have been a single rupture, recent model simulations indicate that a multiple rupture sequence could also explain patterns of subsidence and a trans-Pacific tsunami (42). Successfully dating coseismically killed trees along a greater extent of the CSZ could help distinguish between these single or multiple rupture scenarios to better constrain past CSZ dynamics.

In the Puget Sound region, dendrochronological dating provides the precision necessary to convincingly link events on the Seattle fault zone with those on the Saddle Mountain fault zone. This information can inform updates to current hazard models (43), which are used to set local building code standards, but presently do not consider either the earthquake triggering or multifault earthquake effects that we now identify in the prehistoric record. Including multifault earthquakes will yield larger, more accurate estimates of the maximum magnitude possible (44), and incorporating earthquake clustering effects will improve hazard estimation for short return periods (45, 46), thereby facilitating seismic preparedness and thus safety.

MATERIALS AND METHODS
Dendrochronological data
Wood samples were collected from six sites in the Puget Sound region (Fig. 1) from trees that had previously been radiocarbon dated with uncertainties that span the year 900 CE and were likely killed in an earthquake-related event (8, 16, 18, 21). At each site, we sampled as many trees as possible that retained a fully preserved outermost ring, ideally with bark attached, to return the precise year and season of death. We also sampled trees that experienced decomposition on the outer edge, and although they could not provide a death date, they increased replication and helped extend each site-level chronology as far back in time as possible. All samples included in the analysis are Douglas-fir (*Pseudotsuga menziesii*), and tree-ring measurement data are archived at the National Oceanic and Atmospheric Administration International Tree-Ring Databank (ITRDB; www.ncei.noaa.gov/products/paleoclimatology/

tree-ring) as datasets CAN382 and WA155 to WA160. See table S1 for details on sample sizes and tree-ring data properties at each site.

Price Lake
Located in the Olympic Mountain foothills, Price Lake (lat: 47.471; lon: −123.165; Fig. 1) was formed when the Saddle Mountain fault ruptured, forming an upstream-facing scarp that impounded a stream, thereby submerging the surrounding forest. Stumps in growth position were sampled using an increment borer during a 2005 campaign led by J. Hughes. Another sampling campaign organized by J. Pearl in May 2021 used an increment borer and a Stanley CS11 underwater hydraulic chainsaw to collect samples. We also included samples that had been collected by P. Pringle for radiocarbon dating in an earlier study (8). Twenty-one trees were dated, four with bark (ITRDB dataset WA159; www.ncei. noaa.gov/access/paleo-search/study/38207).

Hamma Hamma
Trees were buried in lake deposits accumulated behind a rockslide-debris avalanche impoundment of John Creek, located on the eastern Olympic Mountain foothills near the delta of the Hamma Hamma River ("Hamma Hamma"; lat: 47.537, lon: −123.066; Fig. 1). Stumps in growth position and subhorizontal logs protruding from lake deposits were sampled by chainsaw and increment borer in 1992, 1997, and 1998 during sampling campaigns led by P. Pringle (8). Seven trees were dated, two with bark (ITRDB dataset WA157; www.ncei.noaa.gov/access/paleo-search/study/38205).

Lake Washington
Trees were deposited to approximately 100 m in depth in Lake Washington ("Lake Washington"; lat: 47.525 lon: −122.234; Fig. 1) as part of a landslide from southeastern Mercer Island. These trees were first removed to ease lake navigation in 1919 and salvaged in 1991 from which slabs were collected by P. Williams, G. Jacoby, and B. Buckley for dendrochronology (21). Tree slabs were acquired for this study from the archives of the Lamont Doherty Earth Observatory Laboratory of Tree-Ring Research (LDEO). Sixteen trees were dated, five with bark (ITRDB dataset WA155; www.ncei.noaa.gov/access/paleo-search/study/38203).

Lake Sammamish
This tree was part of a landslide into southwestern Lake Sammamish near Greenwood Point ("Lake Sammamish"; lat: 47.571; lon: −122.086; Fig. 1) and was sampled on 1 June 1997, in a field expedition led by J. Logan and T. Walsh (8). The single slab, which is bark bearing, was acquired for this study from the archives of the LDEO (ITRDB dataset WA158; www.ncei.noaa.gov/access/paleo-search/study/38206).

West Point
This bark-bearing log with flexible limbs rolled onto a subsided marsh that was being, or just had been, coated with centimeters of sand from a tsunami on the shore of Puget Sound in north Seattle. The tree must have originated from the upland, but whether the tsunami entrained it directly, or whether a slide first carried it into Puget Sound, is unknown (5, 21) ("West Point"; lat: 47.662; lon: −122.436; Fig. 1). The single slab, which is bark bearing, was acquired for this study from the archives of the LDEO (ITRDB dataset WA160; www.ncei.noaa.gov/access/paleo-search/study/38208).

Dry Bed Lake
This site ("Dry Bed"; lat: 47.318, lon: −123.391; Fig. 1) is located in the eastern Olympic Mountain foothills, dammed on its south side

by a rockslide-debris avalanche presumably triggered by earthquake-related shaking. A sample from a single bark-bearing tree was collected by chainsaw in 1992 from a stump in growth position during a sampling campaign led by P. Pringle (8) (ITRDB dataset WA156; www.ncei.noaa.gov/access/paleo-search/study/38204).

MacBlo

For this previously unpublished dataset, Gordon Jacoby collected cores from living and dead old-growth Douglas-fir at a Vancouver Island, British Columbia, site some 280 km northwest of Seattle previously owned by the MacBlo (lat: 49.42, lon: −125.08; Fig. 1 and fig. S3) forestry company. These cores, collected in 1991, were acquired from the LDEO archives and redated and measured by coauthors K. King and G. Harley in 2021. These trees are believed to have been logged soon after collection and more precise locational information is not available. Fifteen trees were dated, nine with bark (ITRDB dataset CAN382; www.ncei.noaa.gov/access/paleo-search/study/38202).

All wood samples were surfaced with increasingly fine sandpaper to 400 grit followed by a final polishing with 30 μm and occasionally 15-μm lapping film. Samples were then imaged on an Epson Expression 12000XL scanner at 2400− or 3200−dots per inch resolution. To capture a complete transect from center to edge, many samples required multiple overlapping scans, which were merged into a single mosaic using the "Photomerge" function in Adobe Photoshop software. Within each site, samples were visually crossdated beginning with samples for which the outermost increment was preserved (23).

In all samples, total ring width was measured using CooRecorder software (24). Multiple transects, usually two, were measured per wood section, while a single transect was typically measured per tree core (table S1). Within each site, crossdating was statistically verified using the program CDendro (24). First, the high-frequency, serially independent component of growth variability was extracted from each measurement time series using the "heavy detrend" option. These patterns were compared between measurement time series using Pearson correlation coefficients and "T values," where

$$T \text{ value} = c \ \sqrt{(n - 2)/(1 - c^2)} \qquad (1)$$

c is Pearson correlation coefficient and n is the number of overlapping years (24). For a given correlation coefficient, the T value decreases as overlap between the two series decreases, which mitigates the chances of spuriously high values when degrees of freedom are low. T values were calculated across all possible lags in time for which there were at least 30 years of overlap between the two series.

Once agreement was verified within trees, each measurement time series was compared to the average of all other series in the accumulating master chronology. A new series was added only if running correlations with the master chronology were strong, positive (Pearson's r correlation coefficient generally between 0.4 and 0.7) and consistent over the length of the series. Second, the new measurement time series was compared to the master chronology across all possible lags with a minimum of at least 30 years overlap. The measurement time series was considered correctly dated if the T value at the given lag was very conspicuously greater than those at all other possible lags.

Once all measurement time series had been added to the dataset, a final statistical check of crossdating was performed using the

program COFECHA (25). In COFECHA, each measurement time series was detrended with a cubic spline of 50% frequency cutoff at 32 years to isolate the high-frequency component of growth. To ensure serial independence and thus meet assumptions of correlation analysis, any remaining autocorrelation was removed using low-order autoregressive functions. Each standardized time series was correlated to the mean of all others in 50-year segments overlapping by 25 years. Any dating errors would frameshift (i.e., temporally offset) the growth pattern in time, causing a conspicuously low correlation (or even negative correlation) in segments that predate the error. The wood of any samples with low correlations was visually reinspected, and measurements were corrected if an error was identified. Site-level master chronologies were compared against one another using CDendro and considered a match if running correlations were positive, strong (>0.4), and consistent over the shared interval. The T value at the lag at which the series was dated must also be very conspicuously greater than those at all other possible lags.

The "MacBlo" Douglas-fir chronology was compared to chronologies developed from samples killed during the earthquake to establish the exact calendar year of death (table S1). There is, however, another long Douglas-fir chronology in the region, which was developed using live-collected samples and dead-collected wood from Heal Lake, BC, Canada (29). The Heal Lake chronology strongly correlates to the mean of Hamma Hamma, Lake Washington, and Price Lake chronologies, yielding a T value (6.8) that is strong and very conspicuously greater than all other possible lags in time. However, the calendar year for the peak 6.8 T value between Heal Lake and the mean of the Hamma Hamma, Lake Washington, and Price Lake chronologies is 1055 CE, 132 years after the 923 CE date established using the MacBlo chronology and independently corroborated by the 774 to 775 CE radiocarbon excursion (Figs. 2 and 3). The reason for this discrepancy may be due to previously unrecognized dating errors in the Heal Lake chronology, which is developed from a large number (n = 150) of relatively short measurement time series (average series length = 164 years) (fig. S3A). As the length of measurement time series decreases, the probability of spurious crossdating matches increases.

To address this issue of apparently spurious crossdating, we attempted to statistically recrossdate the Heal Lake dataset using the original measurement time series and the R package RingDateR (47). We were able to reconstruct the Heal Lake chronology back to about 1400 CE, although without the benefit of using the wood samples to provide additional anatomical features (e.g., fire scars and conspicuously narrow or pronounced latewood) to aid in crossdating. We also developed other earlier "floating" segments of the Heal Lake chronology within which measurement time series crossdate strongly but could not be convincingly linked with one another to yield a continuous, absolutely dated chronology. Thus, we suspect that the mean of Hamma Hamma, Lake Washington, and Price Lake chronologies correlates strongly with a crossdated, well-replicated segment of the Heal Lake chronology, but that segment of the Heal Lake chronology is misplaced in time by 132 years. In contrast, the MacBlo chronology is generated from longer measurement time series (average length = 510 years) with greater overlap among samples, including some measurement time series approximately 1150 years in length (fig. S3B). As further evidence of potential dating problems, the running correlation between the Heal Lake chronology and MacBlo chronology drops sharply in the mid-

1400s CE. Between the mid-1400s CE and 1990 CE, correlations are consistently positive ($r \sim 0.40$ to 0.60), while before the mid-1400s CE, correlations fluctuate around zero (fig. S3C).

Annual radiocarbon

Annual tree rings were dissected from a single dated sample at Lake Washington (SMB036), Hamma Hamma (HH01), and Price Lake (PL06). All radiocarbon sample preparation and analysis were performed at the National Ocean Sciences Accelerator Mass Spectrometer (NOSAMS) facility at the Woods Hole Oceanographic Institution in Woods Hole, MA, USA, where standard high-precision radiocarbon dating methods were applied (48). Briefly, samples were pretreated using a modified "Acid-Base-Acid" method to remove nonstructural carbon and extract cellulose. The pretreated samples were combusted to CO_2 via an elemental analyzer (Costech 4010) and converted to filamentous graphite using standard automated hydrogen reduction graphite procedures before the graphite powders were pressed into aluminum targets and run on the accelerated mass spectrometer.

Samples were normalized to both OX-I and secondary standards (IAEA C-7 and FIRI D) of known ^{14}C ages. Radiocarbon-free potassium hydrogen phthalate (Sigma-Aldrich, P1088) was used for blank correction. Radiocarbon results were calibrated for secular changes in atmospheric radiocarbon concentrations using the International Radiocarbon Calibration Curve (IntCal20) (49). ^{14}C values were converted to Δ^{14}C using Eq. 2

$$\Delta^{14}\text{C} = [Fm * \varepsilon^{\lambda(1950 - Y_c)} - 1] * 1000 \qquad (2)$$

where Fm is the fraction modern, λ is the inverse of the true mean life of radiocarbon, and Y_c is the absolutely dated year. All radiocarbon data from NOSAMS are provided in table S2. Once radiocarbon analysis was complete, we could verify that the rings identified as 774 and 775 CE from dendrochronological dating contained the large single-year jump in Δ^{14}C in each radiocarbon time series.

We also compared measured values with the full range of annual tree-ring ^{14}C data published for the 774 to 775 CE events (30). While the large single-year jump in our data confirms the calendar tree-ring dating and complies with other published records in this respect, the character of the response at our sites is somewhat atypical when compared with several Western North American sites ["West NA"; fig. S4 and (30)]. The differences may be due to the combined effects of a localized (or possible laboratory based) offset in radiocarbon and the moderate climatic conditions at these low elevation sites where the radial growth season is relatively long at approximately 6 months and where trees can periodically photosynthesize during the relatively mild wintertime. The highly consistent response observed in the trees at our three sites is, however, very similar to the response observed in mountain hemlock from Prince William Sound, Alaska (USA10; fig. S4), also published in (30). This provides independent verification of our data and underscores the possibility that responses to the 774 to 775 CE events may be more varied in sites outside those traditionally targeted for dendroclimatic reconstruction.

Likelihood of an asynchronous earthquake doublet versus a single multifault rupture

We can use aftershock statistics and earthquake-size scaling to estimate the relative probabilities of 1) serial earthquakes on the Seattle

fault zone and Saddle Mountain fault zone, versus 2) a single, larger, multifault earthquake. For the serial-earthquake scenario, we used the median magnitude estimates calculated by Styron and Sherrod (11) of a M_w 7.5 earthquake on the Seattle fault zone and a M_w 7.3 earthquake on the Saddle Mountain fault zone, occurring within 6 months of each other. Because aftershocks are usually smaller in magnitude than the mainshock, it is more likely that the M_w 7.5 earthquake triggered the M_w 7.3 earthquake than the other way around. Given a M_w 7.5 mainshock, we estimate the probability of a $M_w \geq 7.3$ aftershock using the Reasenberg and Jones model (50), which estimates the rate of aftershocks above magnitude M_{aft} with time t since a magnitude M_{main} mainshock as

$$\lambda(t) = 10^{a + b(M_{main} - M_{aft})}(t + c)^{-p}$$

Here a, b, c, and p are constants describing the size, productivity, and temporal scaling of aftershocks. We use parameters fit to global onshore subduction-zone regions (51), namely, $a = -2.02$, $b = 1$, $c = 0.018$, and $p = 0.81$. We integrate $\lambda(t)$ over a 6-month period to obtain the expected number N of aftershocks; the Poisson probability of one or more aftershocks is then given by $1 - e^{-N}$. This calculation gives a 16% chance for the two-earthquake scenario, conditional on the M_w 7.5 earthquake.

For the single, multifault earthquake scenario, our preferred magnitude is the median M_w 7.8 as calculated by Styron and Sherrod (11). Here, we can use the Gutenberg-Richter earthquake-size scaling law (52) to estimate the relative probability of an earthquake reaching $M_w \geq 7.8$, provided that it is at least M_w 7.5. The number of earthquakes above M_w is proportional as 10^{-bM}, where b is approximately 1. Therefore, an ongoing earthquake, having already generated seismic moment equivalent to a M_w 7.5 earthquake, has a 50% chance (i.e., $10^{-7.8}/10^{-7.5}$) of reaching at least $M_w \geq 7.8$ in final size.

We can thus estimate that while both the serial earthquake scenario and the multifault earthquake scenario are possible, the multifault earthquake is approximately three times as likely, a value that changes minimally if the window is narrowed to 150 days (3.2 times more likely) or widened to 210 days (3.0 times more likely) in the event of an anomalously short or long 923 to 924 CE dormant period. Note that in this calculation, we have used our preferred magnitudes. However, this calculation is dependent on the relative magnitudes of the scenarios, which are uncertain. For example, if the multifault rupture scenario has a M_w of 7.7 (which is consistent with adding the areas of M_w 7.5 and M_w 7.3 earthquakes), then the multifault earthquake is four times as likely. It is a general result, however, that doublet scenarios are less likely than single multifault earthquakes with conserved rupture area (e.g., if the doublet scenario had identically sized earthquakes, instead of differing by 0.2 magnitude units as with our preferred estimates, the multifault earthquake is five times as likely as the doublet). This is because Gutenberg-Richter scaling implies higher probabilities for rupture growth than Omori scaling implies for triggering (i.e., $b = 1$ implies that an earthquake has a 50% probability of doubling in rupture area, whereas most aftershock sequences have a largest aftershock that is much smaller than the mainshock).

The calculations above are based on well-understood aftershock and earthquake size scaling laws. They do not consider, for example, the effects of the fault geometries involved. In the case of the Seattle fault zone and Saddle Mountain fault zone, while we have shown

that events on these faults are related, we do not know if these faults are physically connected (and they don't need to be physically connected for rupture on one fault to affect the hazard on the other). Furthermore, the exact details of the fault geometry may have different effects for different triggering mechanics (e.g., on dynamic versus static triggering), and these effects are poorly understood. Our simple calculation based on statistical scaling laws does not, however, depend on these triggering mechanisms nor does it require a better resolution of the fault geometry.

Supplementary Materials
This PDF file includes:
Figs. S1 to S5
Tables S1 and S2

REFERENCES AND NOTES

1. D. E. Goldberg, T. Taymaz, N. G. Reitman, A. E. Hatem, S. Yolsal-Çevikbilen, W. D. Barnhart, T. S. Irmak, D. J. Wald, T. Öcalan, W. L. Yeck, B. Özkan, J. A. Thompson Jobe, D. R. Shelly, E. M. Thompson, C. B. DuRoss, P. S. Earle, R. W. Briggs, H. Benz, C. Erman, A. H. Doğan, C. Altuntaş, Rapid characterization of the February 2023 Kahramanmaraş, Türkiye, earthquake sequence. *Seism. Rec.* **3**, 156–167 (2023).

2. S. Kusumoto, K. Imai, T. Hori, Time difference between the 1854 CE Ansei–Tokai and Ansei–Nankai earthquakes estimated from distant tsunami waveforms on the west coast of North America. *Prog. Earth Planet. Sci.* **9**, 2 (2022).

3. N. J. Litchfield, P. Villamor, R. J. V. Dissen, A. Nicol, P. M. Barnes, D. J. A. Barrell, J. R. Pettinga, R. M. Langridge, T. A. Little, J. J. Mountjoy, W. F. Ries, J. Rowland, C. Fenton, M. W. Stirling, J. Kearse, K. R. Berryman, U. A. Cochran, K. J. Clark, M. Hemphill-Haley, N. Khajavi, K. E. Jones, G. Archibald, P. Upton, C. Asher, A. Benson, S. C. Cox, C. Gasston, D. Hale, B. Hall, A. E. Hatem, D. W. Heron, J. Howarth, T. J. Kane, G. Lamarche, S. Lawson, B. Lukovic, S. T. McColl, C. Madugo, J. Manousakis, D. Noble, K. Pedley, K. Sauer, T. Stahl, D. T. Strong, D. B. Townsend, V. Toy, J. Williams, S. Woelz, R. Zinke, Surface rupture of multiple crustal faults in the 2016 Mw 7.8 Kaikōura, New Zealand, Earthquake. *Bull. Seismol. Soc. Am.* **108**, 1496–1520 (2018).

4. M. P. Tuttle, E. S. Schweig, J. D. Sims, R. H. Lafferty, L. W. Wolf, M. L. Haynes, The earthquake potential of the New Madrid seismic zone. *Bull. Seismol. Soc. Am.* **92**, 2080–2089 (2002).

5. B. F. Atwater, Geologic evidence for earthquakes during the past 2000 years along the Copalis River, southern coastal Washington. *J. Geophys. Res. Solid Earth* **97**, 1901–1919 (1992).

6. R. C. Bucknam, E. Hemphill-Haley, E. B. Leopold, Abrupt uplift within the past 1700 years at southern Puget Sound, Washington. *Science* **258**, 1611–1614 (1992).

7. R. E. Karlin, S. E. B. Abella, A history of Pacific Northwest earthquakes recorded in Holocene sediments from Lake Washington. *J. Geophys. Res. Solid Earth* **101**, 6137–6150 (1996).

8. R. L. Logan, R. L. Schuster, P. T. Pringle, T. J. Walsh, S. P. Palmer, Radiocarbon ages of probable coseismic features from the Olympic Peninsula and Lake Sammamish, Washington. *Washington Geology* **26**, 59–67 (1998).

9. R. L. Schuster, R. L. Logan, P. T. Pringle, Prehistoric rock avalanches in the Olympic Mountains, Washington. *Science* **258**, 1620–1621 (1992).

10. B. Sherrod, J. Gomberg, Crustal earthquake triggering by pre-historic great earthquakes on subduction zone thrusts. *J. Geophys. Res. Solid Earth* **119**, 1273–1294 (2014).

11. R. H. Styron, B. Sherrod, Improving paleoseismic earthquake magnitude estimates with rupture length information: Application to the Puget lowland, Washington state, U.S.A. *Bull. Seismol. Soc. Am.* **111**, 1139–1153 (2021).

12. A. R. Nelson, S. F. Personius, B. L. Sherrod, H. M. Kelsey, S. Y. Johnson, L. A. Bradley, R. E. Wells, Diverse rupture modes for surface-deforming upper plate earthquakes in the southern Puget Lowland of Washington State. *Geosphere* **10**, 769–796 (2014).

13. R. E. Wells, C. S. Weaver, R. J. Blakely, Fore-arc migration in Cascadia and its neotectonic significance. *Geology* **26**, 759–762 (1998).

14. B. F. Atwater, A. L. Moore, A tsunami about 1000 years ago in Puget Sound, Washington. *Science* **258**, 1614–1617 (1992).

15. B. F. Atwater, Radiocarbon dating of a Seattle earthquake to A.D. 900-930. *Seismol. Res. Lett.* **70**, 232 (1999).

16. B. L. Sherrod, Evidence for earthquake-induced subsidence about 1100 yr ago in coastal marshes of southern Puget Sound, Washington. *Geol. Soc. Am. Bull.* **113**, 1299–1311 (2001).

17. B. L. Sherrod, T. M. Brocher, C. S. Weaver, R. C. Bucknam, R. J. Blakely, H. M. Kelsey, A. R. Nelson, R. Haugerud, Holocene fault scarps near Tacoma, Washington, USA. *Geology* **32**, 9–12 (2004).

18. E. A. Barnett, B. L. Sherrod, J. F. Hughes, H. M. Kelsey, J. L. Czajkowski, T. J. Walsh, T. A. Contreras, E. R. Schermer, R. J. Carson, Paleoseismic evidence for late holocene tectonic deformation along the Saddle Mountain fault zone, southeastern Olympic Peninsula, Washington. *Bull. Seismol. Soc. Am.* **105**, 38–71 (2015).

19. R. J. Blakely, B. L. Sherrod, J. F. Hughes, M. L. Anderson, R. E. Wells, C. S. Weaver, Saddle Mountain fault deformation zone, Olympic Peninsula, Washington: Western boundary of the Seattle uplift. *Geosphere* **5**, 105–125 (2009).

20. J. R. Wilson, M. J. Bartholomew, R. J. Carson, Late Quaternary faults and their relationship to tectonism in the Olympic Peninsula, Washington. *Geology* **7**, 235–239 (1979).

21. G. C. Jacoby, P. L. Williams, B. M. Buckley, Tree ring correlation between prehistoric landslides and abrupt tectonic events in Seattle, Washington. *Science* **258**, 1621–1623 (1992).

22. D. K. Yamaguchi, B. F. Atwater, D. E. Bunker, B. E. Benson, M. S. Reid, Tree-ring dating the 1700 Cascadia earthquake. *Nature* **389**, 922–923 (1997).

23. M. A. Stokes, T. L. Smiley, *An Introduction to Tree-Ring Dating.* (The University of Arizona Press, Tucson, Arizona, ed. 2, 1996), 73 pp.

24. L. Larsson, *CDendro Programs of the CooRecorder/CDendro Package Version 8.1.* (Saltsjobaden, Sweden, 2013). https://www.cybis.se/forfun/dendro/prgintro/index.htm.

25. R. L. Holmes, Computer-assisted quality control in tree-ring dating and measurement. *Tree-Ring Bull.* **43**, 69–78 (1983).

26. W. H. Emmingham, Comparison of selected Douglas-fir seed sources for cambial and leader growth patterns in four western Oregon environments. *Can. J. For. Res.* **7**, 154–164 (1977).

27. S. J. Grillos, F. H. Smith, The secondary phloem of Douglas-fir. *For. Sci.* **5**, 377–388 (1959).

28. C. Harrington, K. Ford, B. St. Clair, Phenology of Pacific Northwest tree species. *Tree Planters' Notes* **59**, 76–85 (2016).

29. Q.-B. Zhang, R. J. Hebda, Abrupt climate change and variability in the past four millennia of the southern Vancouver Island, Canada. *Canada. Geophys. Res. Lett.* **32**, L16708 (2005).

30. U. Büntgen, L. Wacker, J. D. Galván, S. Arnold, D. Arseneault, M. Baillie, J. Beer, M. Bernabei, N. Bleicher, G. Boswijk, A. Bräuning, M. Carrer, F. C. Ljungqvist, P. Cherubini, M. Christl, D. A. Christie, P. W. Clark, E. R. Cook, R. D'Arrigo, N. Davi, Ó. Eggertsson, J. Esper, A. M. Fowler, Z. Gedalof, F. Gennaretti, J. Grießinger, H. Grissino-Mayer, H. Grudd, B. E. Gunnarson, R. Hantemirov, F. Herzig, A. Hessl, K. U. Heussner, A. J. T. Jull, V. Kukarskih, A. Kirdyanov, T. Kolář, P. J. Krusic, T. Kyncl, A. Lara, C. LeQuesne, H. W. Linderholm, N. J. Loader, B. Luckman, F. Miyake, V. S. Myglan, K. Nicolussi, C. Oppenheimer, J. Palmer, I. Panyushkina, N. Pederson, M. Rybníček, F. H. Schweingruber, A. Seim, M. Sigl, O. Churakova, J. H. Speer, H. A. Synal, W. Tegel, K. Treydte, R. Villalba, G. Wiles, R. Wilson, L. J. Winship, J. Wunder, B. Yang, G. H. F. Young, Tree rings reveal globally coherent signature of cosmogenic radiocarbon events in 774 and 993 CE. *Nat. Comm.* **9**, 3605 (2018).

31. F. Miyake, K. Nagaya, K. Masuda, T. Nakamura, A signature of cosmic-ray increase in AD 774-775 from tree rings in Japan. *Nature* **486**, 240–242 (2012).

32. C. Oppenheimer, L. Wacker, J. Xu, J. D. Galván, M. Stoffel, S. Guillet, C. Corona, M. Sigl, N. Di Cosmo, I. Hajdas, B. Pan, R. Breuker, L. Schneider, J. Esper, J. Fei, J. O. S. Hammond, U. Büntgen, Multi-proxy dating the 'Millennium Eruption' of Changbaishan to late 946 CE. *Quat. Sci. Rev.* **158**, 164–171 (2017).

33. J. K. Pearl, K. J. Anchukaitis, J. P. Donnelly, C. Pearson, N. Pederson, M. C. Lardie Gaylord, A. P. McNichol, E. R. Cook, G. L. Zimmermann, A late Holocene subfossil Atlantic white cedar tree-ring chronology from the northeastern United States. *Quat. Sci. Rev.* **228**, 106104 (2020).

34. D. Eberhart-Phillips, P. J. Haeussler, J. T. Freymueller, A. D. Frankel, C. M. Rubin, P. Craw, N. A. Ratchkovski, G. Anderson, G. A. Carver, A. J. Crone, T. E. Dawson, H. Fletcher, R. Hansen, E. L. Harp, R. A. Harris, D. P. Hill, S. Hreinsdóttir, R. W. Jibson, L. M. Jones, R. Kayen, D. K. Keefer, C. F. Larsen, S. C. Moran, S. F. Personius, G. Plafker, B. Sherrod, K. Sieh, N. Sitar, W. K. Wallace, The 2002 Denali Fault earthquake, Alaska: A large magnitude, slip-partitioned event. *Science* **300**, 1113–1118 (2003).

35. M. J. Rymer, Triggered surface slips in the Coachella Valley associated with the 1992 Joshua Tree and Landers, California, Earthquakes. *Bull. Seismol. Soc. Am.* **90**, 832–848 (2000).

36. J. Lin, R. S. Stein, M. Meghraoui, S. Toda, A. Ayadi, C. Dorbath, S. Belabbes, Stress transfer among en echelon and opposing thrusts and tear faults: Triggering caused by the 2003 Mw 6.9 Zemmouri, Algeria, earthquake. *J. Geophys. Res. Solid Earth* **116**, B03305 (2011).

37. M. Stewart, "Scenario for a magnitude 6.7 earthquake on the Seattle fault" (Earthquake Engineering Research Institute and the Washington Military Department, Emergency Management Division, 2005), 32 pp.

38. A. Dolcimascolo, D. W. Eungard, C. Allen, R. J. LeVeque, L. M. Adams, D. Arcas, V. V. Titov, F. I. González, C. Moore, Tsunami inundation, current speeds, and arrival times simulated from a large Seattle Fault earthquake scenario for Puget Sound and other parts of the

Salish Sea, *Washington State Geology*, Map Series 2022-03, 16 sheets, scale 1:48,000, 7 July 2022.

39. G. C. Jacoby, P. R. Sheppard, K. E. Sieh, Irregular recurrence of large earthquakes along the San Andreas Fault: Evidence from trees. *Science* **241**, 196–199 (1988).

40. J. Watt, D. Ponce, T. Parsons, P. Hart, Missing link between the Hayward and Rodgers Creek faults. *Sci. Adv.* **2**, e1601441 (2016).

41. G. C. Jacoby, D. E. Bunker, B. E. Benson, Tree-ring evidence for an A.D. 1700 Cascadia earthquake in Washington and northern Oregon. *Geology* **25**, 999–1002 (1997).

42. D. Melgar, Was the January 26th, 1700 Cascadia earthquake part of a rupture sequence? *Earth* **126**, e2021JB021822 (2021).

43. A. Frankel, R. Chen, M. Petersen, M. Moschetti, B. Sherrod, Update of the Pacific Northwest portion of the U.S. National Seismic Hazard Maps. *Earthq. Spectra* **31**, S131–S148 (2014, 2015).

44. M. T. Page, More fault connectivity is needed in seismic hazard analysis. *Bull. Seismol. Soc. Am.* **111**, 391–397 (2020).

45. E. H. Field, K. R. Milner, N. Luco, The seismic hazard implications of declustering and Poisson assumptions inferred from a fully time-dependent model. *Bull. Seismol. Soc. Am.* **112**, 527–537 (2021).

46. S. Wang, M. J. Werner, R. Yu, How well does Poissonian Probabilistic Seismic Hazard Assessment (PSHA) approximate the simulated hazard of epidemic-type earthquake sequences? *Bull. Seismol. Soc. Am.* **112**, 508–526 (2021).

47. D. J. Reynolds, D. C. Edge, B. A. Black, RingdateR: A Statistical and graphical tool for crossdating. *Dendrochronologia* **65**, 125797 (2021).

48. B. E. Longworth, K. F. Von Reden, P. Long, M. L. Roberts, A high output, large acceptance injector for the NOSAMS Tandetron AMS system. *Nucl. Instrum. Methods Phys. Res.* **361**, 211–216 (2015).

49. P. J. Reimer, W. E. N. Austin, E. Bard, A. Bayliss, P. G. Blackwell, C. Bronk Ramsey, M. Butzin, H. Cheng, R. L. Edwards, M. Friedrich, P. M. Grootes, T. P. Guilderson, I. Hajdas, T. J. Heaton, A. G. Hogg, K. A. Hughen, B. Kromer, S. W. Manning, R. Muscheler, J. G. Palmer, C. Pearson, J. Van Der Plicht, R. W. Reimer, D. A. Richards, E. M. Scott, J. R. Southon, C. S. M. Turney, L. Wacker, F. Adolphi, U. Büntgen, M. Capano, S. M. Fahrni, A. Fogtmann-Schulz, R. Friedrich, P. Köhler, S. Kudsk, F. Miyake, J. Olsen, F. Reinig, M. Sakamoto, A. Sookdeo, S. Talamo, The IntCal20 Northern Hemisphere radiocarbon age calibration curve (0-55 cal kBP). *Radiocarbon* **62**, 725–757 (2020).

50. P. A. Reasenberg, L. M. Jones, Earthquake hazard after a mainshock in California. *Science* **243**, 1173–1176 (1989).

51. M. T. Page, N. van der Elst, J. L. Hardebeck, K. Felzer, A. J. Michael, Three ingredients for improved global aftershock forecasts: Tectonic region, time-dependent catalog incompleteness, and intersequence variability. *Bull. Seismol. Soc. Am.* **106**, 2290–2301 (2016).

52. B. Gutenberg, C. F. Richter, Frequency of earthquakes in California. *Bull. Seismol. Soc. Am.* **34**, 185–188 (1944).

A multifault earthquake threat for the Seattle metropolitan region revealed by mass tree mortality

Bryan A. Black, Jessie K. Pearl, Charlotte L. Pearson, Patrick T. Pringle, David C. Frank, Morgan T. Page, Brendan M. Buckley, Edward R. Cook, Grant L. Harley, Karen J. King, Jonathan F. Hughes, David J. Reynolds, and Brian L. Sherrod

View the article online
https://www.science.org/doi/10.1126/sciadv.adh4973
Permissions
https://www.science.org/help/reprints-and-permissions

Use of this article is subject to the Terms of service